Preparation of the Large-Mode-Area Ytterbium-Doped Microstructure Fibre and Laser Performance

Zhou Dechun[1] Bai Xuemei[1] Zhou Hang[2]

[1] *School of Materials Science and Engineering, Changchun University of Science and Technology, Changchun, Jilin* 130022, *China*

[2] *School of Electric Power, South China University of Technology, Guangzhou, Guangdong* 510640, *China*

Abstract The waveguide structure of the large-mode microstructure fiber is designed in view of the efficient coupling and laser output quality during the practical application of the high-power fiber laser. It employs the bundle drawing technology to prepare the ytterbium-doped microstructure fibre with the core diameter of 41 μm, inner-cladding numerical aperture of 0.62, core numerical aperture of 0.05 and effective mode area of 530 μm^2. The output power of the single-mode laser is 19.1 W, the slope efficiency is 55.2% and the beam quality factor of M^2 is less than 1.01, on the condition that the pump power is 35.0 W.

Key words fiber optics; ytterbium-doped microstructure fibre; large-mode-area; bundle drawing; laser performance

OCIS codes 060.2290; 060.5295; 060.2280; 060.2270

大模场面积掺镱微结构光纤的制备与激光性能

周德春[1] 白雪梅[1] 周 航[2]

([1] 长春理工大学材料科学与工程学院, 吉林 长春 130022; [2] 华南理工大学电力学院, 广东 广州 510640)

摘要 针对高功率光纤激光器在实际应用过程中所面临的高效耦合及激光输出质量问题,自行设计了大模场微结构光纤的波导结构,采用集束拉丝技术制备了纤芯直径 41 μm、内包层数值孔径 0.62、纤芯数值孔径 0.05、有效模场面积约 530 μm^2 的掺镱微结构光纤。在抽运功率为 35.0 W 的条件下,获得的单模激光输出功率为 19.1 W,斜率效率为 55.2%,光束质量因子 M^2 小于 1.01。

关键词 光纤光学; 掺镱微结构光纤; 大模场面积; 集束拉丝; 激光性能

中图分类号 TN253 **文献标识码** A **doi**: 10.3788/CJL201441.1205006

1 Introduction

Ordered microstructure fibre, which has the performances of the large-mode-area and single endless mode operation, can overcome the nonlinear optical effect caused by the high-power laser and implement the low-loss single-mode transmission[1-2]. The excellent characteristics of the ordered microstructure fibre provide the new techonology paths to the high-power high-brilliance fibre lasers and have become one of the most vibrant research fields and a current hot topic[3-5].

At present, there is hysteresis in the research of the rare earth doped microstructure fibre materials in China, which shows in preparation of the small-mode-area of photon crystal fibre (PCF) and its testing techonology, the research of the high-performance rare earth doped microtructure fibre is still in its infancy[6-8]. Therefore, it's of important theoretical and practical meaning for improving high-power fibre laser technology to develop the large-mode-area high-transmission power microstructure fibre materials with intellectual property rights.

The paper proposes the ytterbium-doped microstructure fibre of larger mode area with the improved ion vapor deposition technology and bundle drawing method. It also analyse and evaluates the end structure, spectrum characteristics and laser

收稿日期: 2014-06-15; **收到修改稿日期**: 2014-07-15

基金项目: 国家自然科学基金(61308051)

作者简介: 周德春(1964—),男,博士,副教授,主要从事光纤材料与器件方面的研究。

E-mail: zhoudechun0912@cust.edu.cn

performance with the detection methods by scanning electron microscope and spectrophotometer.

2 Structure design of the large-mode-area microstructure fibre

2.1 Design principle

The microstructure fiber is numerically analyzed with the full-vector effective index method and the cutoff wavelength of the single-mode operation is investigated, which provides a solution to the structure design of the large-mode-area microstructure fibre[9-11]. For the microstructure fiber, the normalized transmission frequency of V_{PCF} can be presented as[12-13]

$$V_{PCF}(\lambda) = \frac{2\pi\Lambda}{\lambda}(n_{core}^2 - n_{eff}^2)^{1/2}, \quad (1)$$

where, n_{core} and n_{eff} identify the equivalent refractive index of the core and cladding respectively, and λ is the wavelength, Λ is the air hole distance in the cladding. When λ converges towards zero, the mode distribution of the transmitted light is nearly fixed. Which is not dependent on the λ and Λ, and will be determined by the relative dimension of the hole aperture in the cladding or the ratio of the Λ to λ. When the normalized transmission frequency of V_{PCF} is less than the constant of π, the single-mode transmission will be maintained.

2.2 Structure design and numerical simulation of the microstructure fibre

The designed microstructure fibre consists of the ytterbium-doped core, inner cladding with ordered array of micro air hole and the outer cladding with closed array of large air hole. It is numerically simulated as the formula (1). According to the different ratio of the d to Λ, where d is the diameter of the inner cladding air hole. Fig. 1 shows the relationship between the normalized cut-off frequency of V_{PCF} and the wavelength of λ. The refractive index of the core and inner cladding are 1.4580 and 1.4397 respectively when wavelength is 1.03 μm. When the ratio of d to Λ does not exceed 0.3, the second-order normalized transmission frequency of the V_{PCF} will be less than π and the single-mode transmission in the microstructure fiber can be implemented.

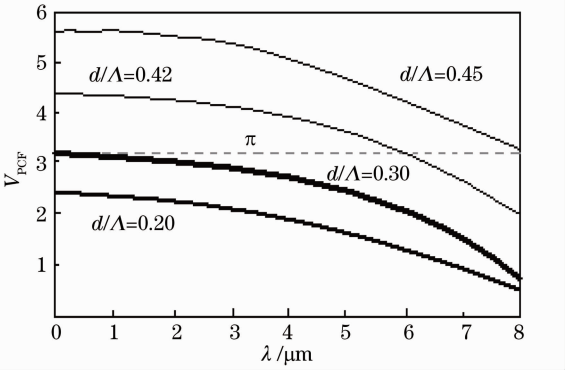

Fig. 1 Relationship between the V_{PCF} and wavelength

3 Preparation of the ytterbium-doped microstructure fibre and its performance experiment

3.1 Preparation of the ytterbium-doped microstructure fibre

In the first place, the improved rare earth ion vapor deposition technology is employed to prepare the ytterbium-doped quartz fibre preform with large core radium. It is implemented at the temperature of about 850 ℃. Ytterbium choloride vapor is channeled to the deposition system and reacts with the oxygen to produce the rare earth material. Simultaneously, high concentration ytterbium ion is doped evenly as a certain proportion mixed air with the gas flow control method to solve the high concertation cluster problem of the rare earth ion solution doped technology, which improves the laser performance of the ytterbium-doped microstructure fibre.

In the second place, silica capillary and the ytterbium-doped fibre core with different sizes are bundled as the cladding size to form the microstructure fibre preform.

Finally, one end of the microstructure fibre which preforms assembled is fixed on the drawing machine and the other end is heated in the tube electric furnace to implement drawing by the bundle drawing technique. The temperature field is evenly distributed in the furnace and its temperature is higher than 100 ℃, which can soften the glass. During the drawing, the other end of the fibre is extracted the positive pressure to selectively control the air hole collapsing by adjusting the air pressure inside the air hole, which ensures the cladding air hole roundness and integrity of the geometric accuracy and prevents the silica capillary from deforming or collapsing.

3.2 Performance testing

The end structural configuration of the ytterbium-doped microstructure fibre is observed under the scanning electron microscope of JSA-840 type. The absorption and emission spectrum of the sample are measured under the room temperature with the spectrophotometer of UV360 type made by the Japanese Shimadzu company. The fluorescence spectrum of the sample is measured with model WFY-28 fluorescence spectrophotometer in the room temperature and the excitation wavelength range is between 800 nm and 1200 nm. The high-power laser diode (LD) module with collimated output is employed as the pumping source and the pump wavelength is about 980 nm. The laser′s structure is typical Fabry-Perot cavity and the laser output power is measured when the high-power pumped laser is injected in the ytterbium-doped

microstructure fibre of 6 m length.

4 Analysis and discussion

4.1 Analysis of the end surface structure shape

The picture under the scanning electron microscope (SEM) of the large-mode-area ytterbium-doped microstructure fibre end surface is shown in Fig. 2. The core diameter is 41 μm, the diameter of the inner cladding is 176 μm, the ratio of the d to Λ is 0.3, where d is 3.06 μm and Λ is 10.2 μm, the diameter of the outer cladding is 278 μm, the aperture of the large air hole is about 20 μm, the thickness of the quartz glass bridge among the air holes is about 0.25 μm, the numerical aperture of the inner cladding is 0.62 and the numerical aperture of the core is 0.05. Fig. 2 shows that the structure of the ytterbium-doped microstructure fibre is even and stable, there is no distortion and the ratio of the d to Λ meets the requirements for the single-mode transmission.

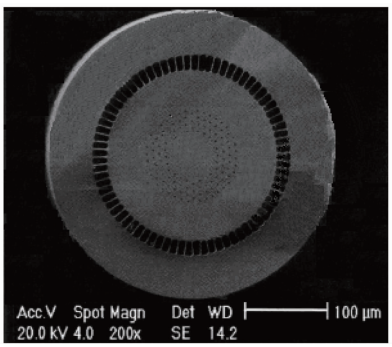

Fig. 2 SEM picture of the ytterbium-doped microstructure fibre end surface

4.2 Analysis of the spectrum performance

4.2.1 Absorption and emission spectrum

The absorption and emission spectrum of the ytterbium-doped microstructure fibre is shown in Fig. 3. The curve of the absorption shows that the range of the Yb^{3+}-absorbed wavelength range is between 850 nm and 1050 nm and the two main absorption peaks occur at the wavelength of 915 nm and 975 nm respectively. The absorption peak is wider at the wavelength of 915 nm and the absorption peak is narrow and sharp at the wavelength of 975 nm. The wide absorption spectrum provides more flexibility for selecting the pumping light source. According to the J-O theory, the absorption section of the Yb^{3+}-doped microstructure fiber is shown below:

$$\sigma_{abs}(\lambda) = \frac{1}{NL}\ln\frac{I_0(\lambda)}{I(\lambda)}, \tag{2}$$

where, N is the concentration of the ytterbium ion, L is the length of the measured sample, $I_0(\lambda)$ is the initial incoming light intensity and $I(\lambda)$ is the light intensity through the measured sample. From the formula (2) and Fig. 3, it can be seen that the second-highest absorption peak lies in the central wavelength of 915 nm and its absorption section is 5.65×10^{-21} cm^2 and the highest absorption peak lies in the wavelength of 975 nm with the absorption section of 2.72×10^{-20} cm^2.

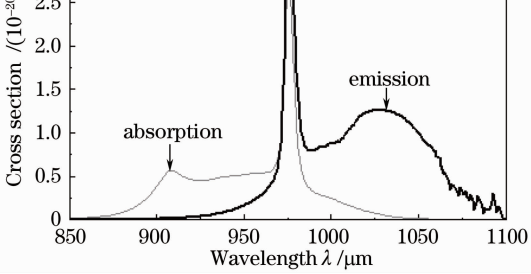

Fig. 3 Absorption and emission section of the ytterbium-doped microstructure fibre

In addition, the emission curve in the Fig. 3 shows that the emission spectrum of Yb^{3+} in the glass base covers from 900 nm to 1100 nm and there are two emission peaks at wavelength of 975 nm and 1030 nm. The emission peak is steeper at the wavelength of 975 nm and the energy level transition corresponds to three-energy-level system, from a to d and e. The emission peak is wider at the wavelength of 1030 nm and the energy level transition corresponds to four-energy-level system, from a to b, d and e. According to McCumber theory, the excited emission section of σ_{emi} is shown below:

$$\sigma_{emi} = \sigma_{abs}\cdot\exp[(E-hc/\lambda)/KT], \tag{3}$$

where, E is the energy difference between $^2F_{7/2}$ and $^2F_{5/2}$, T is the temperature, h is the Planck's constant, c is the light velocity through vacuum and k is the Boltzmann constant. According to the formula (3) and Fig. 3, we can get that the emission section peak for the central wavelength of 975 nm is 3.36×10^{-20} cm^2 and the emission section of the wavelength of 1030 nm is smaller, that is only 1.25×10^{-20} cm^2, while its covered spectrum range is very wide. The emission peak and transmission peak coincides at the wavelength of 975 nm, which will decrease the pumping efficiency of the laser for 975 nm-wavelength. If laser of 980 nm-wavelength is employed, the pumping efficiency will be changed markedly with the wavelength and the amplified spontaneous emission of the 975 nm-wavelength will be restrained effectively.

4.2.2 Fluorescence spectrum

The fluorescence spectrum of the ytterbium-doped microstructure fibre is shown in Fig. 4. There are two fluorescence peaks which are located in 975 nm-wavelength and 1030 nm-wavelength, corresponding to the energy level transition from $^2F_{5/2}$ to $^2F_{7/2}$ in the wavelength range between 900nm and 1100nm. From Fig. 3 and Fig. 4, it is found that the fluorescence peak coincides with the absorption peak and the transmission

peak at the wavelength of 975 nm. Therefore, the fluorescence capture effect will occur in the wave band and the laser cannot output. The laser can output only at the wave band of 1030 nm, where its transmission spectrum is extend to the wavelength of 1100 nm, the effective fluorescence line width is 69.88 nm and the fluorescence lifetime is 950 ms.

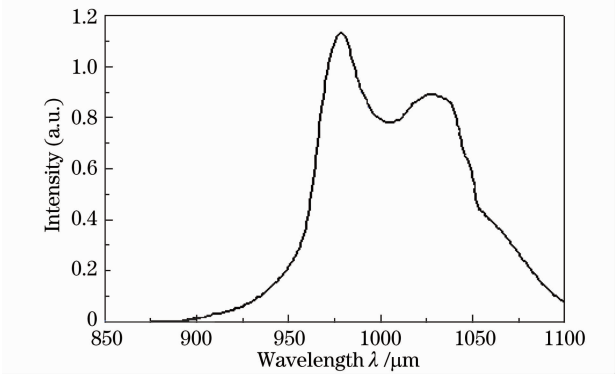

Fig. 4 Fluorescence spectrum of the ytterbium-doped microstructure fibre

4.3 Analysis of the laser characteristic

4.3.1 Energy distribution of the laser beam

Fig. 5 shows the laser beam energy distribution at the wavelength of 1030 nm for the large-mode-area ytterbium-doped microstructure fibre. According to the Fig. 5, the spot approximates to the hexagon, the light field is limited in the core field and in the Gaussian distribution, the effective mode area is 530 μm^2 and the quality factor of M^2 is less than 1.01. Consequently, the ytterbium-doped microstructure fibre has excellent single-mode characteristics when the core diameter is 41 μm and the hole-pitch is 10.2 μm.

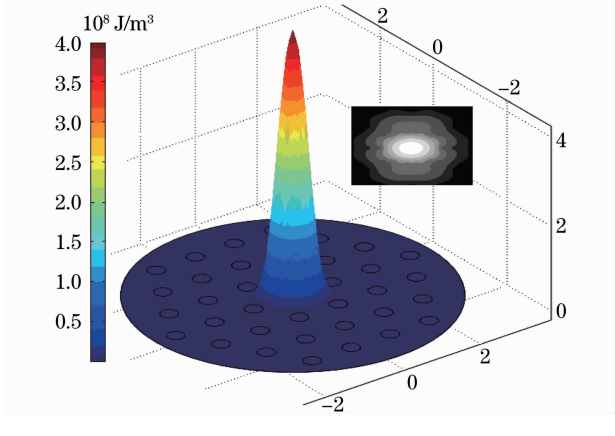

Fig. 5 Energy distribution of the laser beam section

4.3.2 Laser output power analysis and evaluation

The output characteristic of the ytterbium-doped cladding-pumping microstructure fibre laser is researched in the Febry-Perot cavity composed of the dichroscope and the fibre end. The relationship between the laser output power and the input pumping power is shown in Fig. 6. The experiment results show that the laser can output when the input pumping power is higher than 2.13 W. The maximum output power is 19.1 W, the slope efficiency is 55.2% and the spectrum peak of the output laser is near the 1030 nm-wavelength when the pumping power is 35.0 W. The output power has a good linear relation with the input pumping power. There is no saturation when the output power gets the maximum of 19.1 W and the laser spectrum is narrow line width single mode laser. Therefore, we can conclude that the fibre laser has excellent properties.

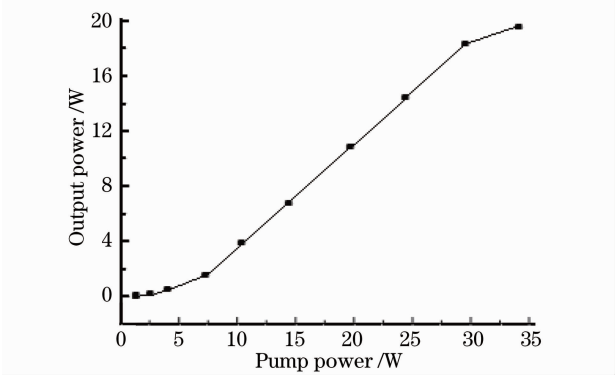

Fig. 6 Output power curve of the ytterbium-doped photonic crystal fibre laser

5 Conclusion

1) The waveguide structure of the large-mode-area ytterbium-doped microstructure fibre with the duty rate of 0.3 is designed due to microstructure fibre's characteristic of single endless mode operation. The large-mode-area ytterbium-doped microstructure fibre with the core diameter of 41 μm and the inner cladding numerical aperture of 0.62 is prepared with the bundle drawing technique.

2) The spectrum performance of the large-mode-area ytterbium-doped microstructure fibre sample is tested. The absorption section is 2.72×10^{-20} cm^2 when the main absorption peak is 975 nm-wavelength. The absorption efficiency will be improved with such large absorption section. At the wavelength of 1030 nm, the emission section is 1.25×10^{-20} cm^2 and the effective fluorescence line width is 69.88 nm and the fluorescence lifetime is 950 ms. The wavelength tuning with 100 nm-wide can be implemented due to the wide emission spectrum range of the wave band.

3) The laser characteristic of the large-mode-area ytterbium-doped microstructure fiber sample with 6 m-length is researched. When the pumping power is 35.0 W, the single-mode output power is 19.1 W, the slope efficiency is 55.2% and the light beam quality factor of M^2 is less than 1.01 at the wavelength of near 1030 nm.

Reference

1 P Russell. Photonic crystal fibers[J]. Science, 2003, 299(5605): 358 - 362.

2 N A Mortensen. Effective area of photonic crystal fibers[J]. Opt

Express, 2002, 10(7): 341 - 348.

3 J Limpert, T Schreiber, A Liem, *et al*.. High-power air-clad large-mode-area photonic crystal fiber laser[J]. Opt Express, 2003, 11(7): 818 - 823.

4 Zhou Dechun, Yu Fengxia, Lu Jingjuan, *et al*.. Design of Yb-doped all-fiber laser device based on optical fiber gratings resonator[J]. Acta Photonia Sinica, 2010, 39(3): 389 - 392.
周德春, 于凤霞, 卢敬娟, 等. 基于光纤光栅谐振腔的掺镱全光纤激光器设计[J]. 光子学报, 2010, 39(3): 389 - 392.

5 J Limpert, T Schreiber, A Liem, *et al*.. Thermo-optical properties of air-clad photonic crystal fiber lasers in high power operation[J]. Opt Express, 2003, 11(22): 2982 - 2990.

6 Yu Chongxiu, Yuan Jinhui, Shen Xiangwei. Recent progress of study on photonic crystal fiber[J]. Acta Optica Sinica, 2011, 31(9): 0900139
余重秀, 苑金辉, 申向伟. 光子晶体光纤的研究新进展[J]. 光学学报, 2011, 31(9): 0900139.

7 Zhang Guang, Zhou Qinling, Hu Lili, *et al*.. A large core phosphate photonic crystal fiber made by a stack-and-draw technique[J]. Chinese J Lasers, 2011, 38(1): 0106003.
张 光, 周秦岭, 胡丽丽, 等. 堆积法制作大芯径磷酸盐光子晶体光纤[J]. 中国激光, 2011, 38(1): 0106003.

8 Lou Qihong, Zhou Jun, Zhang Haibo, *et al*.. Recent progress of large core fiber lasers[J]. Chinese J Lasers, 2010, 37(9): 2235 - 2241.
楼祺洪, 周 军, 张海波, 等. 大芯径光纤激光器的新进展[J]. 中国激光, 2010, 37(9): 2235 - 2241.

9 J W Dawson, M J Messerly, R J Beach, *et al*.. Analysis of the scalability of diffraction-limited fiber lasers and amplifiers to high average power[J]. Opt Express, 2008, 16(17): 13240 - 13266.

10 M Aslund, J Canning, S D Jackson, *et al*.. Diffraction in air-clad fibres[J]. Opt Express, 2005, 13(14): 5227 - 5233.

11 F Stutzki, F Jansen, C Jauregui, *et al*.. Non-hexagonal large-pitch fibers for enhanced mode discrimination[J]. Opt Express, 2011, 19(13): 12081 - 12086.

12 N A Mortensen, J R Folkenberg, M D Nielsen, *et al*.. Modal cut off and the V-parameter in photonic crystal fibers[J]. Opt Lett, 2003, 28(20): 1879 - 1881.

13 S G Yang, Y J Zhang, X Z Peng, *et al*.. Theoretical study and experimental fabrication of high negative dispersion photonic crystal fiber with large area mode field[J]. Opt Express, 2006, 14(7): 3015 - 3023.

栏目编辑: 韩 峰